

A FIRST APPLICATION OF THE ALCOCK-PACZYNSKI TEST TO STACKED COSMIC VOIDS

P. M. SUTTER^{1,2,3,4}, GUILHEM LAVAUX^{5,6}, BENJAMIN D. WANDELT^{2,3,1,7}, AND DAVID H. WEINBERG^{4,8}

¹ DEPARTMENT OF PHYSICS, UNIVERSITY OF ILLINOIS AT URBANA-CHAMPAIGN, URBANA, IL 61801

² UPMC UNIV PARIS 06, UMR7095, INSTITUT D'ASTROPHYSIQUE DE PARIS, F-75014, PARIS, FRANCE

³ CNRS, UMR7095, INSTITUT D'ASTROPHYSIQUE DE PARIS, F-75014, PARIS, FRANCE

⁴ CENTER FOR COSMOLOGY AND ASTRO-PARTICLE PHYSICS, OHIO STATE UNIVERSITY, COLUMBUS, OH 43210

⁵ DEPARTMENT OF PHYSICS & ASTRONOMY, UNIVERSITY OF WATERLOO, WATERLOO, ON, N2L 3G1 CANADA

⁶ PERIMETER INSTITUTE FOR THEORETICAL PHYSICS, WATERLOO, ON, N2L 2Y5, CANADA

⁷ DEPARTMENT OF ASTRONOMY, UNIVERSITY OF ILLINOIS AT URBANA-CHAMPAIGN, URBANA, IL 61801

⁸ DEPARTMENT OF ASTRONOMY, OHIO STATE UNIVERSITY, COLUMBUS, OH 43210

Draft version September 10, 2018

ABSTRACT

We report on the first application of the Alcock-Paczynski test to stacked voids in spectroscopic galaxy redshift surveys. We use voids from the Sutter et al. (2012) void catalog, which was derived from the Sloan Digital Sky Survey Data Release 7 main sample and luminous red galaxy catalogs. The construction of that void catalog removes potential shape measurement bias by using a modified version of the ZOBOV algorithm and by removing voids near survey boundaries and masks. We apply the shape-fitting procedure presented in Lavaux & Wandelt (2012) to ten void stacks out to redshift $z = 0.36$. Combining these measurements, we determine the mean cosmologically induced “stretch” of voids in three redshift bins, with 1σ errors of 5-15%. The mean stretch is consistent with unity, providing no indication of a distortion induced by peculiar velocities. While the statistical errors are too large to detect the Alcock-Paczynski effect over our limited redshift range, this proof-of-concept analysis defines procedures that can be applied to larger spectroscopic galaxy surveys at higher redshifts to constrain dark energy using the expected statistical isotropy of structures that are minimally affected by uncertainties in galaxy velocity bias.

Subject headings: cosmology: observations, cosmology: large-scale structure of universe, cosmology: cosmological parameters, methods: data analysis

1. INTRODUCTION

Characterizing the nature and history of dark energy is perhaps the greatest challenge in the near future of observational cosmology. Many elementary probes now strive to distinguish a cosmological constant from alternative theories of dynamical dark energy or modified gravity. Most probes rely on “standard candles,” such as Type Ia supernovae (e.g., Aldering et al. 2002), or “standard rulers,” such as radio galaxy diameters (Daly et al. 2009) or baryon acoustic oscillations (BAO) (e.g., Eisenstein et al. 2005; Blake et al. 2011; Beutler et al. 2011; Anderson et al. 2012; Mehta et al. 2012). Reviews of dark energy probes, current constraints and forecasts for future experiments include Linder (2003), Albrecht et al. (2006), Frieman et al. (2008), and Weinberg et al. (2012).

Over 30 years ago Alcock & Paczynski (1979, hereafter AP) proposed an elegant alternative approach based on a hypothetical population of idealized spheres. Their key insight was that since galaxy spatial positions are inferred from both their angular positions *and* redshifts, these spheres will appear anisotropic if one adopts an incorrect spacetime metric. Specifically, because line-of-sight distances scale with the inverse Hubble parameter $H^{-1}(z)$ and transverse distances scale with the angular diameter distance $D_A(z)$, their ratio, or *stretch*, measures the value of the product $H(z)D_A(z)$. In practice, the AP test requires only *statistical* isotropy of the observed structures, so the test can be implemented with measures of quasar, galaxy, or Ly α forest clustering, or

features in the redshifted 21 cm spectrum (e.g., Hui et al. 1999; McDonald & Miralda-Escudé 1999; Eriksen et al. 2005; Nusser 2005; Kim & Croft 2007; Blake et al. 2011; Reid et al. 2012). In this paper we apply the AP test to the Sutter et al. (2012) catalog of voids in the galaxy redshift surveys of the Sloan Digital Sky Survey (SDSS; York et al. 2000).

To date, most applications of the AP test have focused on the autocorrelation function or power spectrum (e.g., Ballinger et al. 1996; Matsubara & Suto 1996; Matsubara 2004). Specifically, the clearest detections of the AP effect have been found in the two-point correlations of galaxies in the WiggleZ survey (Blake et al. 2011) and the Baryon Oscillation Spectroscopic Survey (Reid et al. 2012). A successful application of the AP test requires handling the large systematic uncertainties caused by peculiar motions, which introduce redshift-space anisotropy that must be disentangled from the AP effect itself. Uncertainties in the peculiar velocity corrections limit the Blake et al. (2011) and Reid et al. (2012) studies to large, quasi-linear scales, where the statistical uncertainties are relatively large. An attempt was made recently to apply the AP test to close galaxy pairs (Marinoni & Buzzi 2010), but as Bueno Belloso et al. (2012) point out this method has serious shortcoming due to dynamics at small scales. Additionally, the analysis of Jennings et al. (2012) indicates that this method provides relatively weak constraints.

Cosmic voids provide an attractive alternative for applying the AP test, as first proposed by Ryden (1995)

and discussed extensively by Lavaux & Wandelt (2012). Voids are the large, underdense regions that occupy a large fraction of the volume of the Universe and are a natural consequence of the hierarchical growth of structure (Hausman et al. 1983; Thompson & Gregory 2011). While peculiar velocities modestly affect void shapes (Ryden & Melott 1996; Maeda et al. 2011; Lavaux & Wandelt 2012), voids avoid the regions of high velocity dispersion that have such a large impact on the redshift-space correlation function and power spectrum. Indeed, modeling of peculiar velocities in voids is particularly straightforward since they are still in the quasi-linear regime. In addition, the scale of voids is fairly small, with typical comoving radii $\sim 10 h^{-1}\text{Mpc}$ in a densely sampled survey, and they have a large filling factor (i.e., they occupy a majority of the volume of the Universe), amplifying their statistical power relative to other techniques. We can therefore measure the mean void shape with high precision in a large volume survey. Lavaux & Wandelt (2012) showed that a statistics-limited void AP test can dramatically improve the dark energy constraints from the redshift survey planned for the Euclid satellite (Laureijs et al. 2011); the AP test outperforms the BAO constraints from the same survey, even though BAO constraints leverage a known standard ruler, because the scale of the voids is so much smaller than the BAO scale, yielding correspondingly more precise measurements.

We take the void sample for this analysis from the catalog described in (Sutter et al. 2012). That work constructed a void catalog from the main galaxy redshift survey (Strauss et al. 2002) and the luminous red galaxy (LRG) redshift survey (Eisenstein et al. 2001) of the SDSS Seventh Data Release (DR7; Abazajian et al. 2009). We identify voids using a modified version of the Voronoi-based ZOBOV algorithm (Neyrinck 2008). To compensate for the significant Poisson sampling noise in shape measurements of individual voids (Shoji & Lee 2012), we instead measure the mean void shape by “stacking” the galaxy distributions of our identified voids in bins of redshift and radius. The SDSS LRG survey is sparse, so at $z \gtrsim 0.2$ we can only identify large voids, which are limited in number. The combination of moderate redshift leverage and limited statistics prevents us from making a secure detection of the AP effect in this sample, but our proof-of-concept analysis addresses many of the practical issues that will also arise in future data sets at higher redshift.

In the following section we give a brief overview of our method for measuring void shapes and applying the AP test. We review the properties of the Sutter et al. (2012) void catalog in Section 3, followed by a presentation of the stacked voids in Section 4. We estimate the uncertainty in the stretch measurement and present the AP test as applied to our void stacks in Section 5. Finally, we offer concluding remarks and a brief discussion of prospects for future surveys in Section 6.

2. MEASURING VOID STRETCH & THE AP TEST

Our definitions and procedures closely follow those described by Lavaux & Wandelt (2012), who present tests on N-body simulations and forecasts for surveys such as BOSS (Dawson et al. 2012) and Euclid (Laureijs et al. 2011). Given a galaxy’s sky latitude θ , sky longitude

ϕ , and redshift z , we transform to a hybrid coordinate system

$$\begin{aligned} x' &= \frac{cz}{H_0} \cos \phi \cos \theta, \\ y' &= \frac{cz}{H_0} \sin \phi \cos \theta, \\ z' &= \frac{cz}{H_0} \sin \theta, \end{aligned} \quad (1)$$

where c is the speed of light and H_0 is the Hubble parameter at redshift $z = 0$. Note that our coordinate transformation preserves relative distances; in effect, we are performing a slightly modified version of the AP test where we measure shapes directly in redshift space (see Ryden 1995 for a discussion). Since the AP test only applies to two dimensions (the extent along the line of sight and the projected angular extent), we may project positions within the void onto a plane:

$$\begin{aligned} d_v &= \sqrt{x_{\text{rel}}^2 + y_{\text{rel}}^2} \\ z_v &= |z_{\text{rel}}|, \end{aligned} \quad (2)$$

where $(x_{\text{rel}}, y_{\text{rel}}, z_{\text{rel}})$ are the galaxy coordinates relative to the void barycenter \mathbf{X}_v :

$$\mathbf{x}_{\text{rel}} \equiv \mathbf{x}' - \mathbf{X}_v. \quad (3)$$

When stacking voids we place all void barycenters at a common point and rotate the galaxies within each void about a specified axis so that they all share a common line of sight. We then pixelize the density using 10 bins within the maximum void size in that stack, which helps smooth spurious density fluctuations.

For each stacked void, we assume an inner radial profile with form

$$\frac{n(r)}{\bar{n}} = A_0 + A_3 \left(\frac{r}{R_v} \right)^4, \quad (4)$$

where $r = |\mathbf{x}_{\text{rel}}|$, R_v is the void radius (which for our void definition is the effective radius, or the radius of the sphere which has the same volume as the Voronoi-based void volume), \bar{n} is mean galaxy number density within the given sample, and A_0 and A_3 are free parameters. As discussed by (Sutter et al. 2012), due to galaxy bias and Poisson fluctuations caused by the sparseness with which galaxies sample the underlying density distribution the profiles seen in observations are steeper than those in dark matter simulations, so we use a steeper form for a fitted curve. Using this radial profile we fit to an ellipse given by

$$n(d_v, z_v) = \min \left(n_0 + ((d_v/a_d)^2 + (z_v/a_z)^2)^2, n_{\text{max}} \right), \quad (5)$$

where n_0 is the density at the center of the stack, a_d and a_z are the semi-axes along the angular direction and redshift direction, respectively, and n_{max} is a maximum density value. Our fitting procedure requires an estimate of the uncertainty on a per-pixel basis. Our bin smoothing described above allows us to assume that the fluctuations in each pixel are Gaussian with minimal covariance between pixels. We assume with two separate standard deviations depending on the location inside the stack:

$$\sigma(d, z) = \begin{cases} \sigma_0 \sqrt{\frac{1h^{-1}\text{Mpc}}{d_v}}, & \text{if } n(d_v, z_v) < n_{\text{max}} \\ \sigma_1, & \text{otherwise} \end{cases} \quad (6)$$

This gives us a per-pixel sampling uncertainty within the void radius and a fixed standard deviation outside the void. We keep the latter uncertainty fixed because the regions outside the void carry large statistical weight but are largely unimportant to the fit. The factor of $1/d$ accounts for the cylindrical averaging of pixels as we form the stack. The values of σ_0 and σ_1 may be different among different samples, since these give a measure of the relative level of Poisson fluctuations. However, within a sample we expect — and find — that these values are consistent across multiple stacks.

We truncate our stack at $R_{\text{cut}} \equiv 3R_v$. We run a Monte Carlo Markov chain to explore the four parameters of Equation (5), the two standard deviations of Equation (6), and their uncertainties. The likelihood that we must then explore takes the form

$$\chi^2 = \sum_{i=1}^{N_d} \sum_{j=1}^{N_z} \left(\frac{(n(d_i, z_i) - n_{i,j})^2}{\sigma^2(d_i, z_i)} + 2 \log \sigma(d_i, z_i) \right) \quad (7)$$

where N_d is the number of pixels in the angular direction, and N_z is the number of pixels in the redshift direction. The values d_i and z_i are the values of the coordinates d_v and z_v at their respective indices. The exploration of this likelihood gives us both the measurement of the void ellipticity and the overall uncertainty associated with each stack. The analysis of Lavaux & Wandelt (2012) found that the error bars produced from this method were consistent with the level of scatter among independent N-body simulations, though we will conclude below that they underestimate the errors in our data set.

We translate these ellipticities into a cosmological measurement by applying the AP test, in which we measure the ratio of the length along the line of sight to the angular diameter of each stacked void. We will call this ratio the void *stretch*. What follows is a brief discussion of the stretch as a function of redshift; see Lavaux & Wandelt (2012) for a more complete derivation.

We wish to take the ratio of a void length along the line of sight δz_v to its projected angular extent δd_v . In the simple coordinate system of Equation (2), the projected angular extent is related to the angular extent by $\delta d_v \equiv cz\delta\theta/H_0$. The angular extent in turn depends on cosmology via the angular diameter distance $D_A(z)$:

$$\delta\theta = \frac{\delta r_v}{D_A(z)}, \quad (8)$$

where δr_v is the comoving radial extent of the void. In a flat universe, the angular diameter distance is equal to the comoving line of sight distance $D_c(z)$:

$$D_A(z) = D_c(z) = \frac{c}{H_0} \int_0^z \frac{dz'}{E(z')}, \quad (9)$$

where $E(z) \equiv H(z)/H_0$. Combining these gives the expression

$$\delta d = \frac{c}{H_0} \frac{z\delta r_v}{D_A(z)}. \quad (10)$$

The comoving line of sight distance δz_v is also related to $D_c(z)$, and hence $D_A(z)$ in a flat universe, via

$$\delta z_v = \frac{\delta l_v}{dD_A/dz}, \quad (11)$$

where δl_v is the comoving distance along the line of sight. Taking the derivative allows us to identify

$$\delta z_v = \frac{H_0}{c} E(z) \delta l_v. \quad (12)$$

In an isotropic universe a stacked void should have the same extent in all directions; thus, its angular extent should equal its comoving distance along the line of sight. This allows us to assume $\delta l_v = \delta r_v$. Combining Equations (10) and (12) above leads to our desired ratio:

$$\frac{\delta z_v}{\delta d_v} = \left(\frac{H_0}{c} \right)^2 \frac{D_A(z)E(z)}{z}. \quad (13)$$

We identify the void stretch, denoted by $e_v(z)$ for a void at redshift z , as

$$e_v(z) \equiv \frac{c}{H_0} \frac{\delta z_v}{\delta d_v}. \quad (14)$$

We measure this stretch by taking the fitted ellipse parameters of Equation (5) and identifying δz_v as a_z and δd_v as a_d . As we stack voids within redshift bins, we assume that the stack provides a measurement of the *average* stretch in that bin, $\langle \delta z_v / \delta d_v \rangle$, and we will compare that to the average expected stretching in that bin weighted by the void distribution:

$$\bar{e}_v(z) = \frac{1}{N_v} \int_{z_i}^{z_i+\Delta z} e_v(z') N_v(z') dz', \quad (15)$$

where the given bin runs from redshift z_i to Δz , $N_v(z')$ is the number of voids in a given redshift slice, and N_v is the total number of voids in the bin.

Throughout we will assume a flat universe with a cosmological constant, which gives a Hubble equation of

$$E(z, w_0, w_a) = (\Omega_m(1+z)^3 + \Omega_\Lambda)^{1/2}, \quad (16)$$

where Ω_m and Ω_Λ are, respectively, the present-day matter and dark energy densities relative to the critical density.

3. VOID CATALOGS

We take our void catalog from Sutter et al. (2012), which is based on volume-limited samples of the New York University Value-Added Galaxy Catalog (Blanton et al. 2005). This catalog cross-matches galaxies from SDSS (Abazajian et al. 2009) with other surveys using improved photometric calibrations (Padmanabhan et al. 2008). We also use the LRG catalog of Kazin et al. (2010). Table 1 summarizes the volume-limited samples used in this work. Additionally, to improve our statistics by using as many voids as possible, we merge the four samples within $z < 0.2$ into two samples: *dim1+dim2* and *bright1+bright2*. For the smallest and largest voids in each sample these combinations violate our assumption that the voids are evenly distributed throughout each redshift bin. However, we do not use the very largest voids in any case, and the smallest voids have non-uniform redshift distributions within each sample, so we find that this does not strongly affect our results.

Sutter et al. (2012) produced void catalogs using a modified version of the void finder ZOBOV (Neyrinck 2008), which maps the density using Voronoi tessellations (van de Weygaert 2007) and collects these Voronoi

TABLE 1
DATA SAMPLES USED IN THIS WORK.

Sample	Catalog	$M_{r,\min}$	z_{\min}	z_{\max}	Number of Galaxies	Mean Spacing ($h^{-1}\text{Mpc}$)
dim1	NYU VAGC	-18.9	0.0	0.05	63639	3
dim2	NYU VAGC	-20.4	0.05	0.1	156266	5
bright1	NYU VAGC	-21.35	0.1	0.15	113713	8
bright2	NYU VAGC	-22.05	0.15	0.2	43340	13
lrgdim	LRGs	-21.2	0.16	0.36	67567	24
lrgbright	LRGs	-21.8	0.36	0.44	15212	38

cells into zones and voids using a watershed technique (Platen et al. 2007; Aragón-Calvo et al. 2010). This approach naturally identifies a full hierarchy of voids and sub-voids, which we will exploit to capture as many voids as possible. Additionally, the algorithm prevents voids from overlapping. To remove any potential shape measurement bias due to the presence of the mask, we choose the “central” catalog of voids, which are selected such that they could not possibly intersect any boundary or mask in the survey for any given rotation about their barycenters.

4. VOID STACKS

We have many constraints for grouping voids into redshift and radius bins. We choose redshift bins corresponding to the limits of the *dim1+dim2*, *bright1+bright2*, *lrgdim*, and *lrgbright* samples. Within each redshift bin, we divide the voids into bins of radius with the following objectives:

1. *Sufficient numbers* - Within each stack we require enough voids to sufficiently smooth the projected density and increase the signal-to-noise so that we can make reliable measurements. While this number is not fixed, we have found empirically that we require at least ~ 15 voids per stack for the subsequent stretch measurement to converge reliably.
2. *Multiple radial bins* - As many independent measurements within the same redshift bin as possible allows us to account for scatter that can develop in individual measurements by taking uncertainty-weighted averages of these multiple measurements.
3. *Narrowness* - Each stack should have a narrow radial width; otherwise, the density profile will smooth out to the point that our shape fitting routine cannot reliably measure the ellipticity. Also, smaller voids tend to have more Poisson noise and can severely degrade the measurement when combined with larger voids.
4. *Even distribution* - The voids in each stack should be evenly distributed in redshift so that we reliably measure the mean ellipticity without bias.

Given these conditions, we select four stacks from the *dim1+dim2* and *bright1+bright2* samples and two from the *lrgdim* sample. We discard the *lrgbright* sample because there are not enough voids to construct reliable stacks. The void radius is used to assign voids to stacks. While the tessellation procedure gives the *exact* volume for the given sampling, we may be miscalculating the volume due to the sparseness of the sampling itself. However, we will choose sufficiently broad radial

stacks such that this is not a concern. For each sample, our first stack begins at the mean galaxy separation $\bar{d} \equiv \bar{n}_d^{-1/3}$, which we take as the smallest resolvable void (Tikhonov & Karachentsev 2006; Platen et al. 2011). Below $20 h^{-1}\text{Mpc}$ our bins have width $4 h^{-1}\text{Mpc}$; above this we switch to $8 h^{-1}\text{Mpc}$ widths to collect sufficient numbers of voids (the exception to this rule is the smallest stack of the *bright1+bright2* sample, where we extend the width to include enough voids). We treat the *lrgdim* sample slightly differently due to its much poorer resolution, small number of voids, and wide range of void sizes. For this sample we reject the smallest voids and construct one stack with width $16 h^{-1}\text{Mpc}$ and one with width $36 h^{-1}\text{Mpc}$. We do not include the very largest voids in each sample because they are difficult to reliably combine with smaller voids. However, our bins contain over 95% of the voids in each sample, meaning that we are taking almost full advantage of the void information available in each catalog.

Within each stack we rescale the voids to the maximum void size in that stack; i.e, we multiply all positions relative to the void center by $R_v/R_{v,\max}$. This reduces the effects of Poisson scatter within the inner wall of the stacked void, improving our shape estimation. Where we have combined voids from different samples, we normalize the profile of each void to the mean number density of galaxies in the sample before adding it to the stack.

In Figures 1, 2, and 3 we show the one-dimensional radial profiles for each stack in the *dim1+dim2*, *bright1+bright2*, and *lrgdim* samples, respectively. We construct these profiles by measuring the density within thin spherical shells. We also show the radial profiles of individual voids. Each individual void scatters about the mean density of its sample at large radii. It is only the stacked void which asymptotes to the mean (as seen in Sutter et al. 2012). By re-scaling voids, we move galaxies outside the stack maximum radius, lowering the mean of the stack.

We immediately note the steep profiles relative to results from dark matter-only simulations. This is expected due to the effects of Poisson sampling and the biasing of galaxies as tracers of density and justifies our choice of a quartic radial profile for shape fitting. These plots also highlight the necessity of stacking: attempts to measure the ellipticity of individual voids would be nearly impossible. As in the analysis of Sutter et al. (2012), we see that the stacked voids greatly enhance the signal-to-noise and generate qualitatively similar profiles across many void sizes and redshift ranges.

We show the two-dimensional stacks used in our shape-fitting analysis in Figures 4, 5, and 6. As in Lavaux & Wandelt (2012), to improve the signal-to-noise we fold the stacked void about the d -axis and to alleviate the effects of Poisson sampling we discretize the

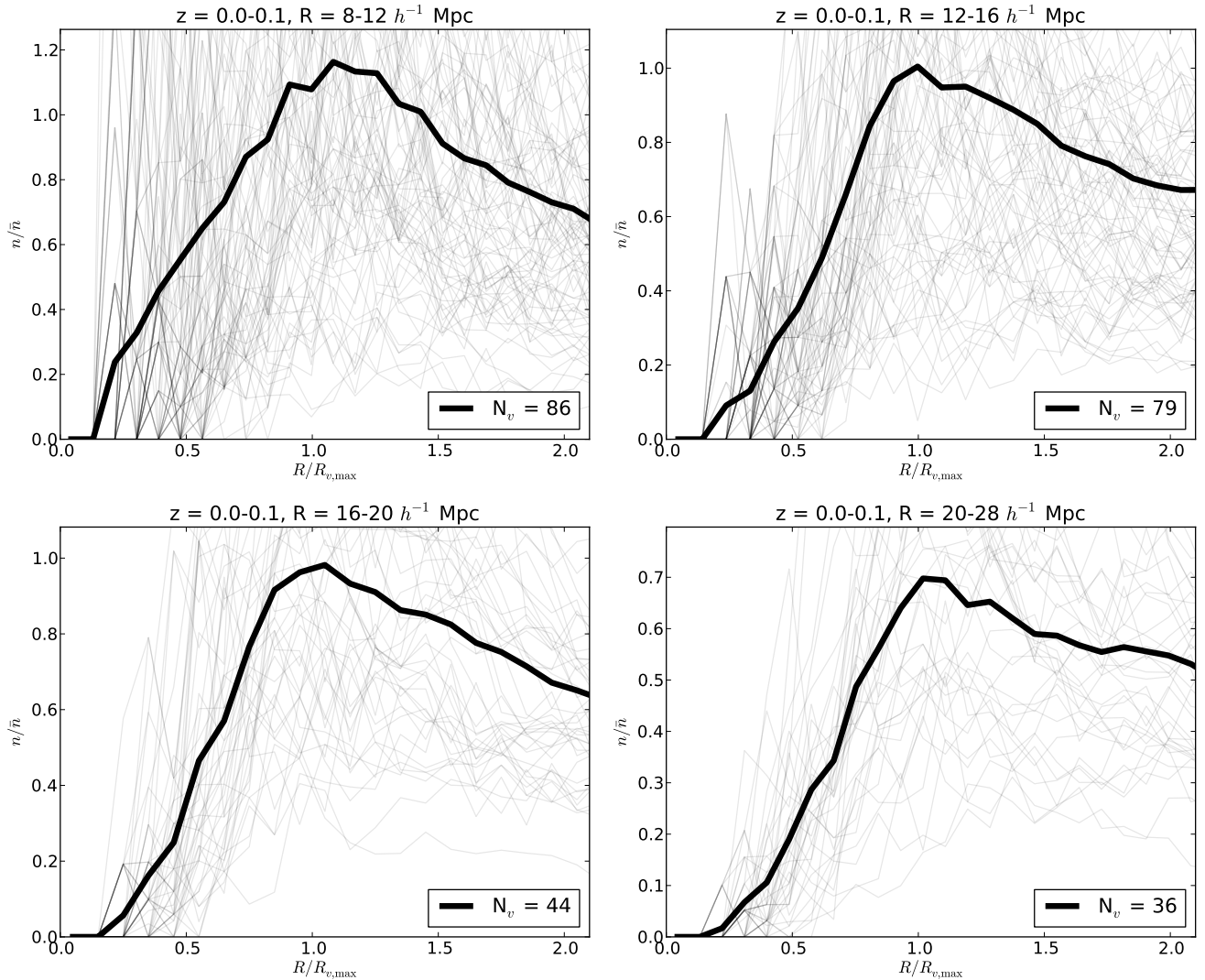


FIG. 1.— *Radial profiles at $0 < z < 0.1$ for the dim+dim2 sample.* We show profiles of individual voids in gray and the profile of the stacked void in black. The legend gives the number of voids in each stack. We rescale each void to the maximum void size within each stack.

density. While Lavaux & Wandelt (2012) used fixed $2 h^{-1}$ Mpc bins for this discretization, our void sizes are much larger, so we choose to scale the bin size with the void radius so that there are always 10 bins within the maximum void radius. For the *lrgdim* sample we widen the pixel size to dampen the larger Poisson noise. The black lines in each plot are the isodensity contours of our best-fit ellipse for each stack using the technique outlined above. The contours stop at the calculated value of n_{max} , which is the mean density outside the void wall. We also list the calculated ratio $\delta z_v / \delta d_v$ in the plot.

Even with our discretization there is still significant variation in the density, especially outside the inner walls of the voids. Additionally, the high-density ridge surrounding the void stack known as the “compensation region” is not clearly defined, since our rescaling of individual voids is designed to clear out the inner regions, which correspondingly widens the compensation region. Fortunately, this does not significantly affect our shape-fitting procedure: by assuming a steep profile, we are most sensitive to the more clearly-defined inner edge of the wall.

Poisson noise and the small number of detected voids make finding a reliable fit in the *lrgdim* samples difficult; we will see that this is reflected in the larger error bars compared to the other samples.

5. VOID STRETCH

Although the fitting procedure defined by Equations (4)-(7) provides an estimate of the uncertainty in each measurement, the method makes rather simple assumptions about the errors in density, namely that they are Gaussian distributed (justifying χ^2 likelihood) with the errors given by Equation (6). This procedure appears to give reasonable statistical errors in the dark matter simulations analyzed by (Lavaux & Wandelt 2012), but here we are analyzing galaxy catalogs, which are sparser and to some degree biased tracers of structure. We have therefore developed an empirical method of estimating errors by creating “incoherent” void stacks: instead of aligning voids within a stack to have a common line of sight, we assign a random set of Euler angles. After rotating each void in this fashion, we align the barycenters and stack the voids as usual. Since we have removed any information about the line of sight by construction, the

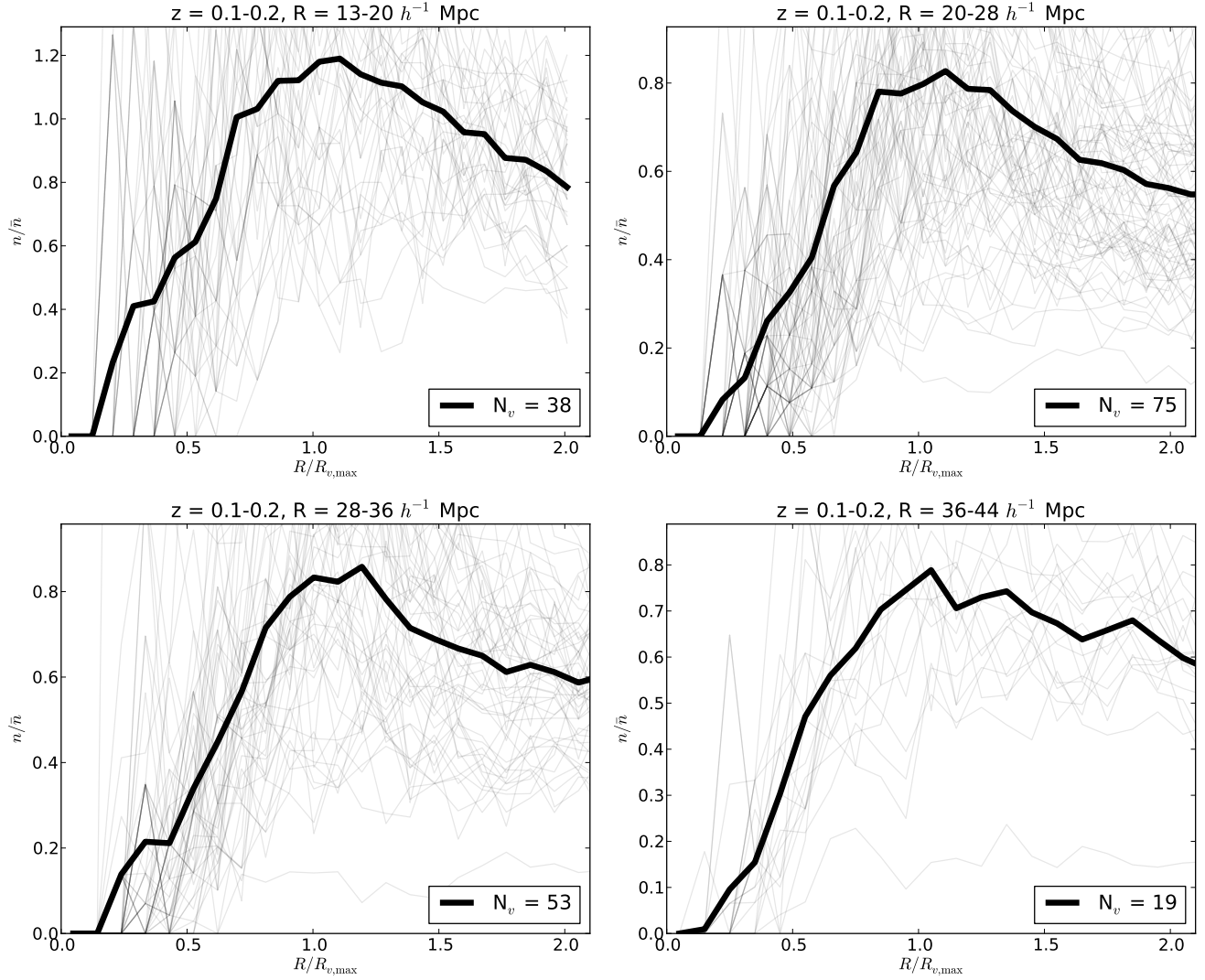


FIG. 2.— Radial profiles at $0.1 < z < 0.2$ for the bright1+bright2 sample. See the caption for Figure 1 for a plot description.

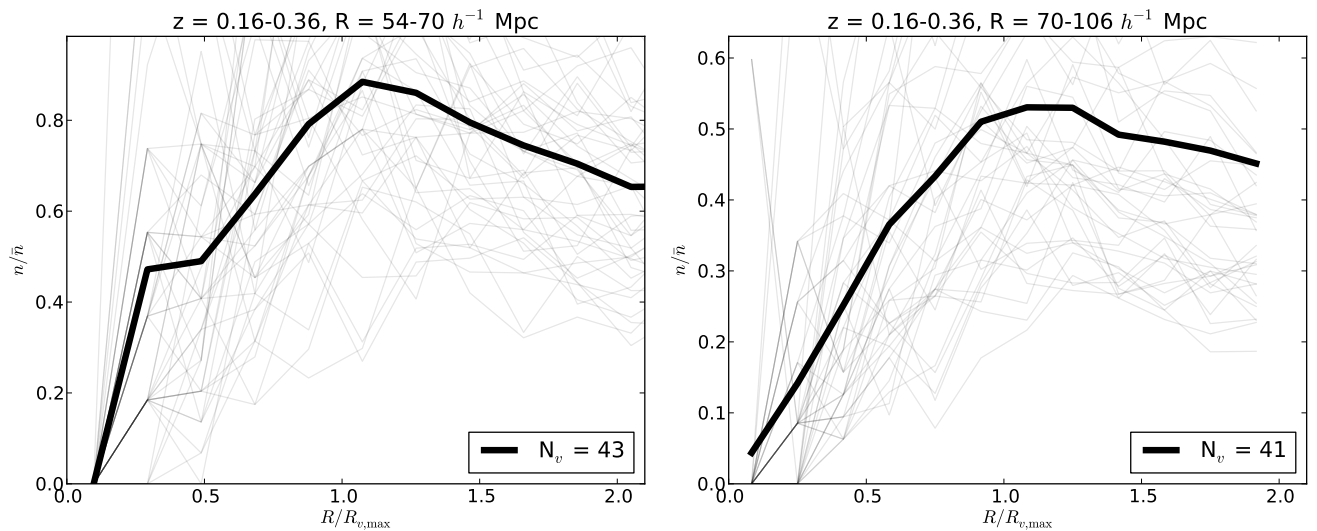


FIG. 3.— Radial profiles at $0.16 < z < 0.36$ for the lrgdim sample. See the caption for Figure 1 for a plot description.

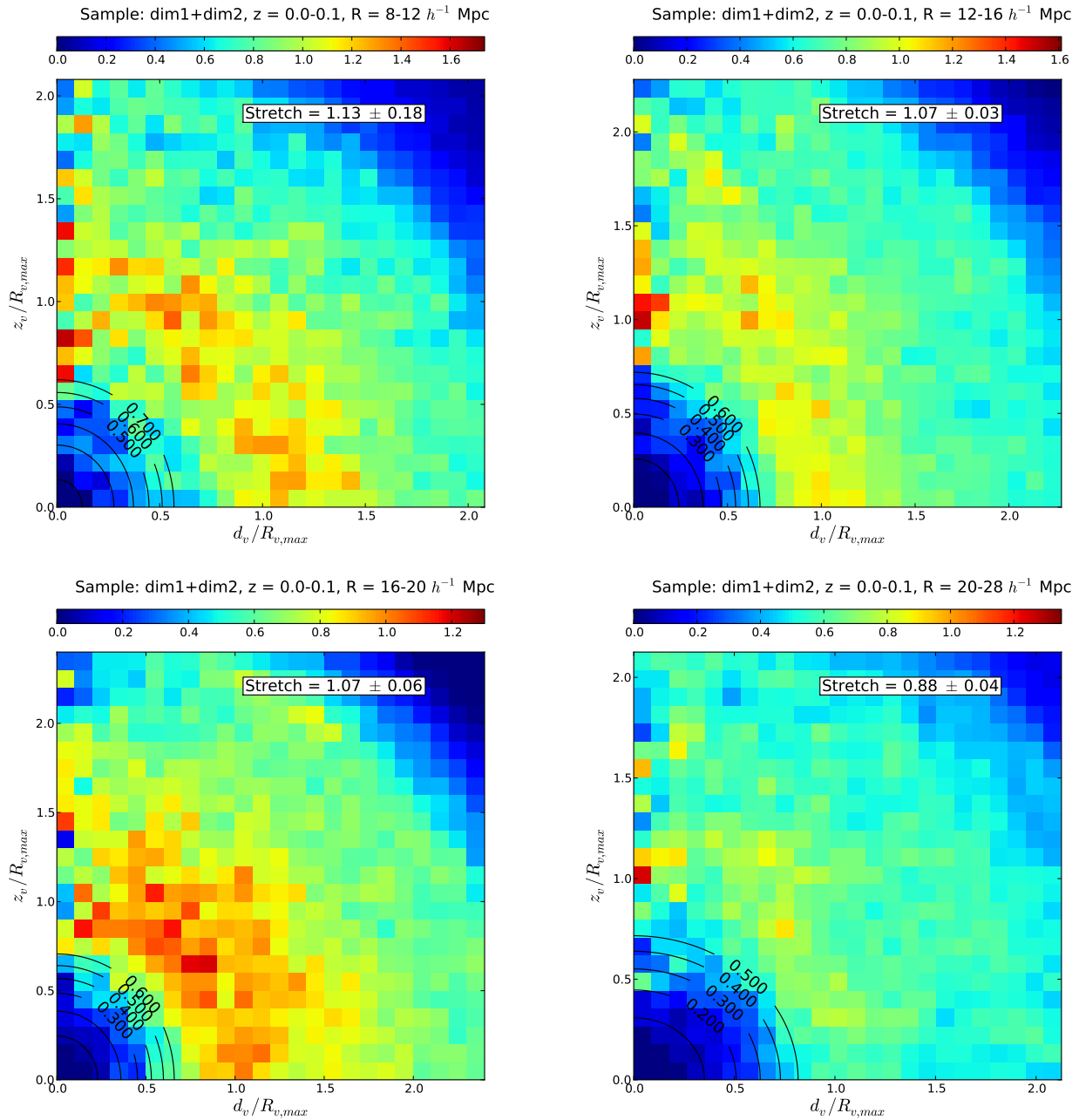


FIG. 4.— *Stacked voids at $0.0 < z < 0.1$ for the dim1+dim2 sample.* Shown are the stacked voids in our hybrid coordinate system (Equation 3). Colors indicate n/\bar{n} , the number density in that bin relative to the mean number density of the sample. The black lines are contours of constant density of our fitted ellipse for each stack, and the text box indicates the measured stretch, or ratio of the length along the line of sight (redshift direction) to the angular extent of the fitted ellipse. The error bars quoted here come directly from the fitting procedure (Equations 5-7).

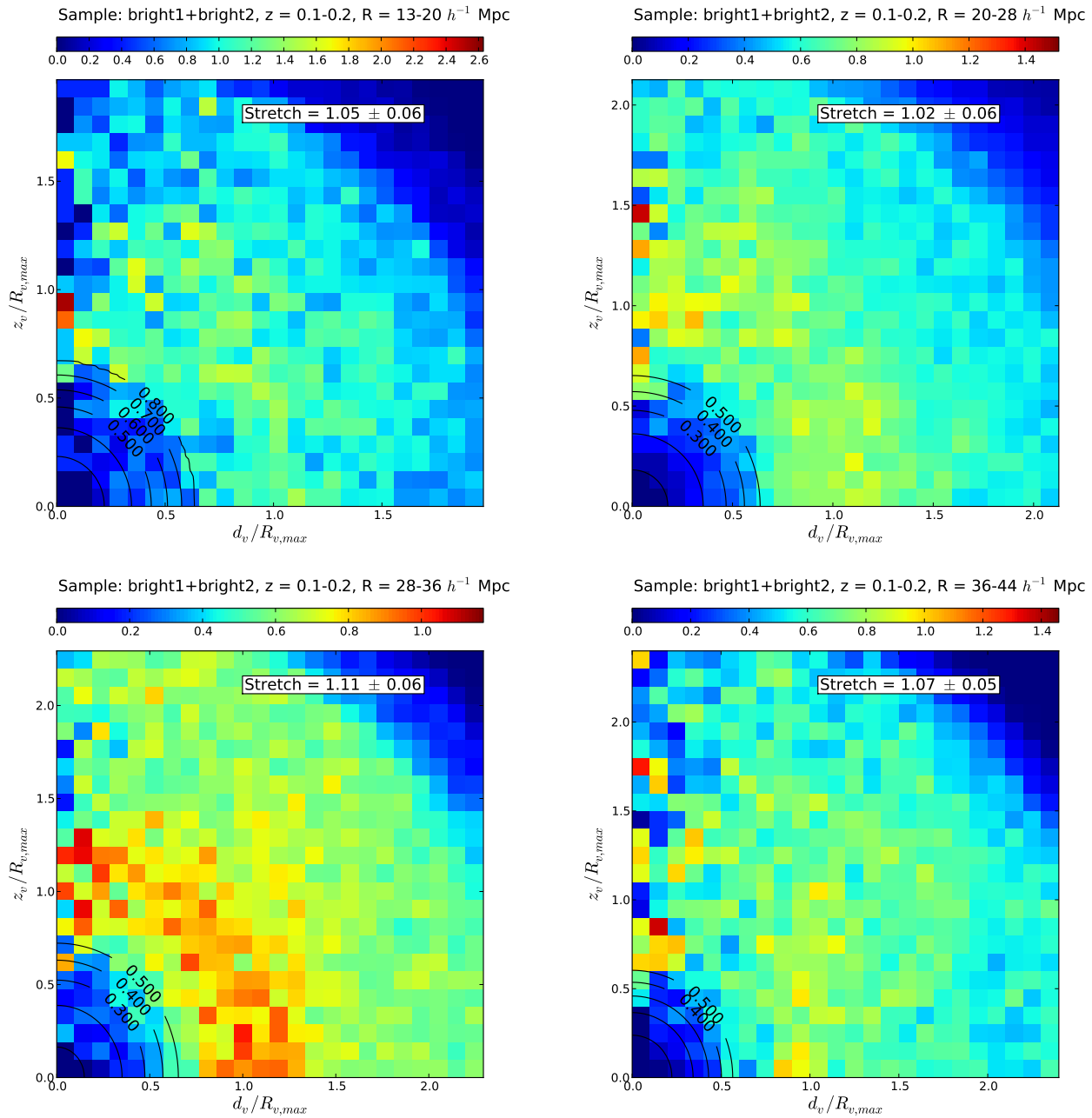


FIG. 5.— *Stacked voids at $0.1 < z < 0.2$ for the bright1+bright2 sample.* See the caption for Figure 4 for a plot description.

mean stretch of the coherent stack must be unity, and the scatter about this value arises from statistical fluctuations that include both the intrinsic scatter in void shapes and the errors in the shape measurements. We create an ensemble of 100 such incoherent stacks, using the same voids in each stack but seeding each new stack with a unique random number seed, and take the rms dispersion of the stretch values as our estimate of the 1σ error.

We may construct diagrams of the measured versus expected void stretch via the identity in Equation (13). Figure 7 shows such a diagram where we collect our stretch measurements from each stack of each sample and compare those to the expected mean stretch in that redshift bin as a function of redshift, $\bar{e}_v(z)$ (Equation 15).

The error bars shown represent the 1σ scatter in the 100 incoherent stacks. For the expected stretch we assume a fiducial cosmology of $\Omega_M = 0.27$, $\Omega_\Lambda = 0.73$, and $h_0 = 0.71$, consistent with the latest WMAP 7-year results combined with supernovae and BAO observations (Komatsu et al. 2011).

There is significant scatter in the *dim1+dim2* sample; this is most likely due to the uneven distribution of voids within the redshift range. We also see significant scatter in the *lrgdim* sample due to the large amount of noise present in the stacked voids. Unfortunately, the statistical errors are too large to detect the expected signal of the AP effect, an increase in stretch from 1.02 in the lowest redshift bin to 1.07 in the highest redshift bin (thick gray bars).

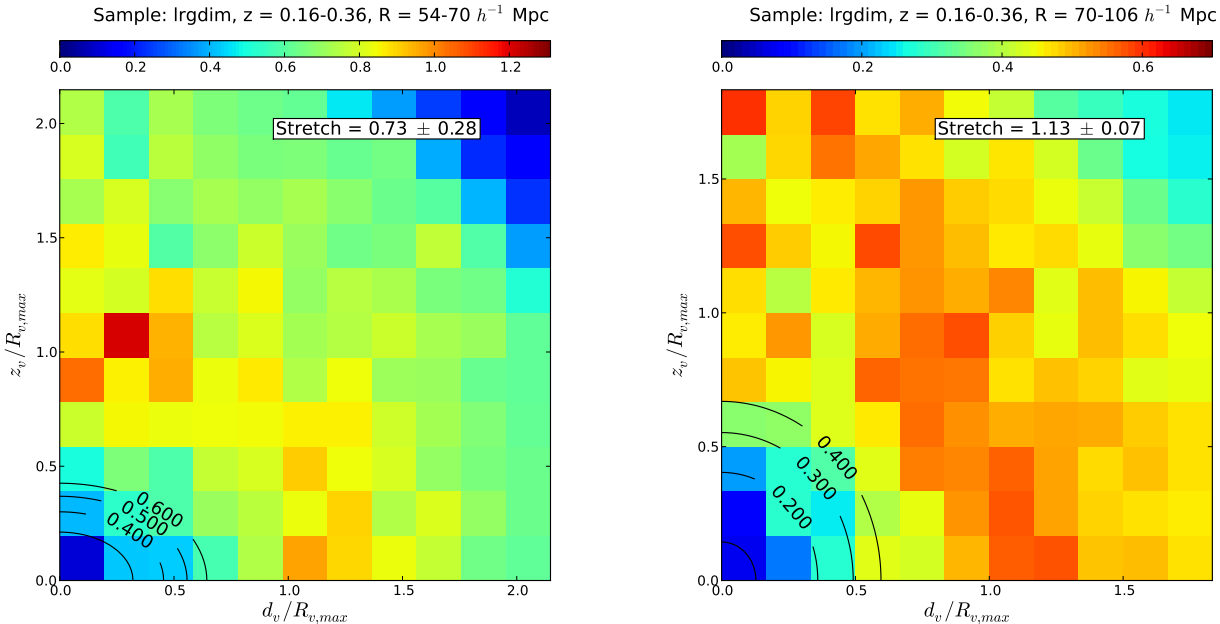


FIG. 6.— *Stacked voids at $0.16 < z < 0.36$ for the lrgdim sample.* See the caption for Figure 4 for a plot description.

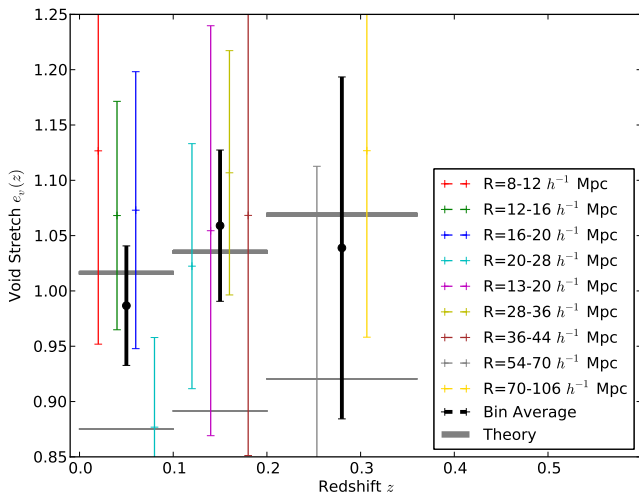


FIG. 7.— *Void stretch as a function of redshift.* We show the measured void stretch (points with error bars) of each stack for all samples versus the expected mean stretch in that redshift bin (thick gray horizontal bands) assuming a cosmology consistent with other recent observations (Komatsu et al. 2011). The thin gray lines indicate the expected stretch including the systematic offset of 16% induced by peculiar velocities that was found in simulations by Lavaux & Wandelt (2012). We assign each radial bin a unique color. Also, the radial bins are ordered left-to-right within each sample redshift range. Note that we distribute the individual points within the redshift range for clarity of plotting only. The black points with error bars indicate the weighted mean of the measurements in that redshift range. Error bars indicate 1σ uncertainty and are derived from an ensemble of incoherent stacks. Note that for clarity we have truncated the mean ellipticity line of the *lrgdim* sample so that it does not overlap the *bright1+bright2* range.

Peculiar velocities have a small but not negligible effect on average void shapes. In N-body tests, Lavaux & Wandelt (2012) find a mean bias of 1.16, with peculiar velocities systematically flattening voids along the line of sight and reducing the stretch factor. Applying this simple factor was all that was necessary to correct for

systematics in their analysis and produce results consistent with expectations. Thin gray lines in Figure 7 show predictions that include this suppression, which actually strongly disagree with our SDSS measurements. However, Lavaux & Wandelt (2012) considered dark matter rather than sparse, biased galaxy tracers, and the voids in their analysis were mostly smaller than the ones in our sample (though somewhat overlapping in size). While correcting for systematics may indeed in the end be “simple”, in terms of only requiring additive or multiplicative factors for a given population of voids, the corrections may be a function of sampling density and void size. Further theoretical work is needed to predict peculiar velocity effects in the regime studied here and evaluate the disagreements with our measurements.

We also performed the same analysis as above but including *all* available voids, including truncated voids near the surveys edges and masks. This also includes all voids which, if rotated, would intersect any edges. The survey boundaries preferentially select voids that lie parallel to them: thus the mask edges will bias our results with an excess of voids parallel to the line of sight, while the redshift boundaries will bias our results with an excess of voids perpendicular to the line of sight. We found that we do not recover a strong positive AP signal, and instead find measurements that scatter around ~ 0.95 . Since the surface area of the spherical cap which defines the redshift boundary is two to three times greater than the surface area of the cone which defines the mask edges, we expect our results to be biased below unity when including all voids. We also increase the scatter in individual measurements due to the inclusion of many smaller and less well-resolved voids. However, with $\sim 30\%$ more voids in each stack we do reduce the error bars for each measurement by a factor of roughly $1/\sqrt{N_v}$.

Figure 8 shows the relative likelihood of Ω_M values in a flat universe with a cosmological constant, given our stretch measurements of SDSS voids. We calculate this

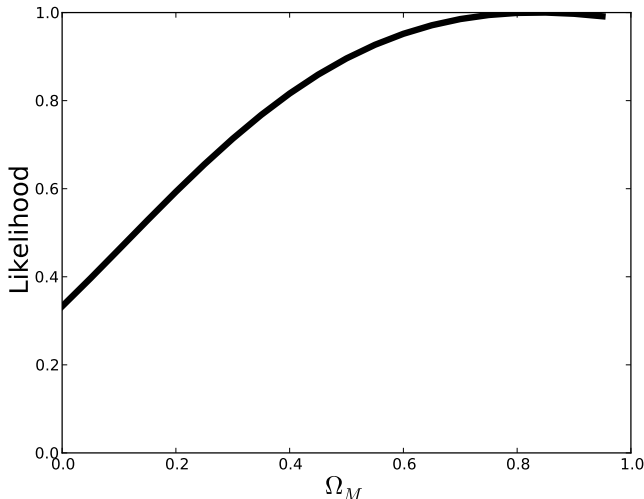


FIG. 8.— *One-dimensional likelihood derived from voids.* We plot the relative likelihood for values of Ω_M in a flat- Λ universe, after marginalizing over a constant peculiar velocity distortion factor in the range 1 – 1.2, assumed to be independent of redshift.

likelihood using the weighted average measurements in each redshift bin (black points in Figure 7), assuming a Gaussian likelihood function. To allow for the effects of peculiar velocities, we marginalize over a constant multiplicative bias factor with a uniform prior in the range [1.0 – 1.2] (the same range of values assumed in the forecasts of Lavaux & Wandelt 2012). A positive detection of the AP effect would correspond to a rejection of $\Omega_M = 0$, since a flat, pure- Λ universe has constant $H(z) = H_0$ and $D_A(z) = cz/H_0$ (i.e., it really does have the coordinate system of Equation 2). As expected from Figure 7, our current statistical errors are too large compared to the predicted stretch signal to detect the AP effect.

6. CONCLUSIONS

We have performed the first application of the Alcock-Paczynski test to stacked voids to observational data. We applied the AP test by measuring ellipticities of stacked voids using the void catalog of Sutter et al. (2012). The stacking procedure greatly reduces the effects of Poisson noise and allows us to reliably apply the shape-fitting algorithm of Lavaux & Wandelt (2012). By grouping voids into multiple radial bins we obtain many independent measurements, and by dividing the void catalog into redshift bins we obtain measurements across the full range of the SDSS DR7 main sample and most of the LRG catalog. However, the limited number of voids and the considerable scatter that remains does not allow us to positively identify the AP effect over the redshift range probed by these data.

The SDSS-III BOSS survey (Dawson et al. 2012) should be a much more powerful basis for void-based AP measurements than the DR7 redshift survey analyzed here. First, in the range of redshift overlap with our *lrgdim* sample ($z = 0.16 - 0.36$), the space density of BOSS galaxies is a factor ~ 3 higher, which enables identification of smaller (and more numerous) voids and more accurate measurement of void density distributions. Second, BOSS extends this higher sampling density out to $z \approx 0.65$, probing a larger comoving volume (and hence more voids) and reaching redshifts where the predicted AP signal is larger, with a

stretch factor $e_V(z = 0.65) = 1.2$ for a flat- Λ universe with $\Omega_M = 0.27$. Future ground-based surveys like BigBOSS (Schlegel et al. 2011) could extend these studies to $z \approx 1$, while the space-based emission line redshift surveys of Euclid (Laureijs et al. 2011) and WFIRST (Green et al. 2011) will probe much larger comoving volumes at $z = 1 - 2.5$. The Fisher matrix analysis of Lavaux & Wandelt (2012) implies that a void-AP analysis of the Euclid survey should yield significantly tighter dark energy constraints than the BAO analysis of the same survey, with a factor of ten improvement in the Dark Energy Task Force (Albrecht et al. 2006) Figure of Merit.

Our initial foray into observational application of this approach highlights two important directions for future investigation. The first is a more detailed study of measurement and parameter fitting procedures and error estimation techniques. Our fitting methods are closely modeled on those of Lavaux & Wandelt (2012), but there may be other approaches that make better use of the available information, such as using an empirical radial profile in place of our adopted parametric model, changing the radial range of the fit, or down-weighting the fluctuations arising from clustered galaxies at the void boundaries. Alternatively, one could avoid profile fitting entirely and instead use anisotropy of the “void-galaxy cross-correlation function,” analogous to the cluster-galaxy cross-correlation but centered at density minima instead of density maxima. The second direction is a more detailed study of peculiar velocity effects on mean void shapes, examining its dependence on void size and on the spatial and velocity bias of galaxy tracers. The likelihood analysis in Figure 8 allows for an overall velocity distortion factor and therefore effectively uses just the redshift dependence of the signal in Figure 7 to constrain cosmology, which was appropriate given the systematic effects noticed in (Lavaux & Wandelt 2012). The goal for future analyses should be to apply a theoretically computed velocity distortion correction to each void sample in each redshift bin and marginalize only over the uncertainty in this correction, getting an absolute constraint on the average void stretch, and hence $H(z)D_A(z)$, at each redshift. In the context of halo occupation distribution (HOD) models (e.g., Zehavi et al. 2011), we expect galaxies to have the same mean velocities as their parent halos on average, but the velocity dispersion of galaxies could differ from that of the dark matter. This velocity dispersion bias can itself be constrained by redshift-space galaxy clustering (Tinker et al. 2006), so we expect the residual uncertainty in peculiar velocity corrections to void shapes to be small, though it may still be the limiting systematic in void-based AP analysis.

The statistical errors of this approach are limited only by the size and redshift range of spectroscopic galaxy surveys, which are expected to grow dramatically in the coming years. Cosmic voids are the converse of galaxy clusters; primordial density minima expand and deepen to form non-linear structures that fill much of the universe and are, in a sense, the most “dark energy dominated” regions of the cosmos. The mean shapes of these regions may ultimately provide powerful clues to the nature of the dark energy that pervades them.

ACKNOWLEDGMENTS

PMS and BDW acknowledge support from NSF Grant AST-0908902. GL acknowledges support from CITA National Fellowship and financial support from the Government of Canada Post-Doctoral Research Fellowship. Research at Perimeter Institute is supported by the Government of Canada through Industry Canada and by the Province of Ontario through the Ministry of Research and Innovation. DW acknowledges support from NSF Grant AST-1009505 and the hospitality of the Institut d’Astrophysique de Paris. This material is based upon

work supported in part by NSF Grant AST-1066293 and the hospitality of the Aspen Center for Physics.

Funding for the Sloan Digital Sky Survey (SDSS) was provided by the Alfred P. Sloan Foundation, the Participating Institutions, the National Aeronautics and Space Administration, the National Science Foundation, the U.S. Department of Energy, the Japanese Monbukagakusho, and the Max Planck Society. The SDSS Web site is <http://www.sdss.org/>.

REFERENCES

- Abazajian, K. N. et al. 2009, *ApJS*, 182, 543
 Albrecht, A. et al. 2006, Report of the Dark Energy Task Force, arXiv:astro-ph/0609591
 Alcock, C. & Paczynski, B. 1979, *Nature*, 281, 358
 Aldering, G. et al. 2002, *Future Research Direction and Visions for Astronomy*. Edited by Dressler, 4835, 146
 Anderson, L. et al. 2012, ArXiv e-prints: 1203.6594
 Aragón-Calvo, M. A., Platen, E., van de Weygaert, R., & Szalay, A. S. 2010, *ApJ*, 723, 364
 Ballinger, W. E., Peacock, J. A., & Heavens, A. F. 1996, *MNRAS*, 282, 877
 Beutler, F. et al. 2011, *MNRAS*, 416, 3017
 Blake, C. et al. 2011, *MNRAS*, 418, 1725
 Blanton, M. R. et al. 2005, *AJ*, 129, 2562
 Bueno Belloso, A., Pettinari, G. W., Meures, N., & Percival, W. J. 2012, *Phys. Rev. D*, 86, 023530
 Daly, R. A., Mory, M. P., O’Dea, C. P., Kharb, P., Baum, S., Guerra, E. J., & Djorgovski, S. G. 2009, *ApJ*, 691, 1058
 Dawson, K. S. et al. 2012, *The Baryon Oscillation Spectroscopic Survey of SDSS-III*, arXiv:1208.0022
 Eisenstein, D. J. et al. 2001, *AJ*, 122, 2267
 Eisenstein, D. J. et al. 2005, *ApJ*, 633, 560
 Eriksen, K. A., Marble, A. R., Impey, C. D., Bai, L., & Petry, C. E. 2005, *Observing Dark Energy*, 339
 Frieman, J. A., Turner, M. S., & Huterer, D. 2008, *Annual Review of A&A*, 46, 385
 Green, J. et al. 2011, *Wide-Field InfraRed Survey Telescope (WFIRST) Interim Report*, arXiv: 1108.1374
 Hausman, M. A., Olson, D. W., & Roth, B. D. 1983, *ApJ*, 270, 351
 Hui, L., Stebbins, A., & Burles, S. 1999, *ApJ*, 511, L5
 Jennings, E., Baugh, C. M., & Pascoli, S. 2012, *MNRAS*, 420, 1079
 Kazin, E. A. et al. 2010, *ApJ*, 710, 1444
 Kim, Y.-R. & Croft, R. A. C. 2007, *MNRAS*, 374, 535
 Komatsu, E. et al. 2011, *ApJS*, 192, 18
 Laureijs, R. et al. 2011, *Euclid Definition Study Report*, arXiv: 1110.3193
 Lavaux, G. & Wandelt, B. D. 2012, *ApJ*, 754, 109
 Linder, E. V. 2003, *Mapping the Dark Energy Equation of State*, arXiv:astro-ph/0311403
 Maeda, K.-i., Sakai, N., & Triay, R. 2011, *JCAP*, 2011, 026
 Marinoni, C. & Buzzi, A. 2010, *Nature*, 468, 539
 Matsubara, T. 2004, *ApJ*, 615, 573
 Matsubara, T. & Suto, Y. 1996, *ApJ*, 470, L1
 McDonald, P. & Miralda-Escudé, J. 1999, *ApJ*, 518, 24
 Mehta, K. T., Cuesta, A. J., Xu, X., Eisenstein, D. J., & Padmanabhan, N. 2012, eprint arXiv:1202.0092
 Neyrinck, M. C. 2008, *MNRAS*, 386, 2101
 Nusser, A. 2005, *MNRAS*, 364, 051027041230005
 Padmanabhan, N. et al. 2008, *ApJ*, 674, 1217
 Platen, E., van de Weygaert, R., & Jones, B. J. T. 2007, *MNRAS*, 380, 551
 Platen, E., van de Weygaert, R., Jones, B. J. T., Vegter, G., & Calvo, M. A. A. 2011, *MNRAS*, 416, 2494
 Reid, B. A. et al. 2012, *MNRAS*, 426, 2719
 Ryden, B. S. 1995, *ApJ*, 452, 25
 Ryden, B. S. & Melott, A. L. 1996, *ApJ*, 470, 160
 Schlegel, D. et al. 2011, *The BigBOSS Experiment*, arXiv:1106.1706
 Shoji, M. & Lee, J. 2012, ArXiv e-prints: 1203.0869
 Strauss, M. A. et al. 2002, *AJ*, 124, 1810
 Sutter, P. M., Lavaux, G., Wandelt, B. D., & Weinberg, D. H. 2012, *A public void catalog from the SDSS DR7 Galaxy Redshift Surveys based on the watershed transform*, arXiv:1207.2524
 Thompson, L. A. & Gregory, S. A. 2011, ArXiv e-prints: 1109.1268
 Tikhonov, A. V. & Karachentsev, I. D. 2006, *ApJ*, 653, 969
 Tinker, J. L., Weinberg, D. H., & Zheng, Z. 2006, *MNRAS*, 368, 85
 van de Weygaert, R. 2007, *Voronoi Tessellations and the Cosmic Web: Spatial Patterns and Clustering across the Universe*, arXiv: 0707.2877
 Weinberg, D. H., Mortonson, M. J., Eisenstein, D. J., Hirata, C., Riess, A. G., & Rozo, E. 2012
 York, D. G. et al. 2000, *AJ*, 120, 1579
 Zehavi, I. et al. 2011, *ApJ*, 736, 59